

Dynamics of Low Anisotropy Morphologies in Directional Solidification

B. Utter* and E. Bodenschatz†

Laboratory of Atomic and Solid State Physics, Cornell University, Ithaca, NY 14853

(Dated: November 8, 2018)

We report experimental results on quasi-two-dimensional diffusion limited growth in directionally solidified succinonitrile with small amounts of poly(ethylene oxide), acetone, or camphor as a solute. Seaweed growth, or dense branching morphology, is selected by growing grains close to the $\{111\}$ plane, where the in-plane surface tension is nearly isotropic. The observed growth morphologies are very sensitive to small anisotropies in surface tension caused by misorientations from the $\{111\}$ plane. Different seaweed morphologies are found, including the degenerate, the stabilized, and the strongly tilted seaweeds. The degenerate seaweeds show a limited fractal scaling range and, with increased undercooling, suggests a transition from “fractal” to “compact” seaweed. Strongly tilted seaweeds demonstrate a significant twofold anisotropy. In addition, seaweed-dendrite transitions are observed in low anisotropy growth.

I. INTRODUCTION

It is well known that surface tension anisotropy plays a crucial role in the formation of cells and dendrites in solidification microstructures [1]. Early on, for isotropic growth, theory found [2] that the speed and tip radius of cellular growth were nonunique, while experiment showed clear selection [3]. The break-through to this puzzle came when it was shown that a small amount of anisotropy acts as a singular perturbation destroying the non-uniqueness of the selected tip [1].

Cells and dendrites have been studied extensively, but the study of nearly isotropic growth in solidification has received less attention. Without anisotropy the growth is characterized by frequent random tip splitting leading to a disordered pattern. This situation has been coined seaweed growth [4] or dense branching morphology (DBM) [5]. Similar patterns are observed in other growth systems which lack anisotropy, most notably viscous fingering (Hele-Shaw flow) [6, 7], but also in such different systems as growth of bacterial colonies [8, 9], electrodeposition [7, 10], annealing of magnetic films [11], and drying water films [12]. In fact, in viscous fingering experiments, it was found that introducing anisotropy can stabilize the tips and induce dendrites [13].

In this article we report experimental results on weakly anisotropic growth in directionally solidified succinonitrile (SCN) with small amounts of poly(ethylene oxide), acetone, or camphor as a solute. As described in Section II, the quasi-2D sample is oriented close to the $\{111\}$ plane leading to a nearly isotropic surface tension. Weak deviations from the $\{111\}$ orientation are found to introduce anisotropies and profoundly affect the tip dynamics of the solidification front. These deviations are expected for experimental solidification studies using model alloys since precise control of sample orientation is not

currently possible. Different types of seaweeds are observed, depending on the weak anisotropy: degenerate seaweeds that can lead to alternating tip splitting [14], stabilized seaweeds, and strongly tilted seaweeds which reveal a large twofold anisotropy.

In addition, we explore the existence of fractal growth in degenerate seaweeds at low speeds and find that seaweeds in directional solidification do not appear to be fractal over a significant range of length scales. We also report results on transitions between seaweed and dendrite growth.

Anisotropy in solidification originates from the capillary length which is proportional to the surface stiffness

$$\tilde{\gamma}(\hat{\mathbf{n}}) = \gamma(\hat{\mathbf{n}}) + \frac{\partial^2 \gamma(\hat{\mathbf{n}})}{\partial \alpha^2} \quad (1)$$

where γ is the surface tension and α is the angle between the normal to the interface $\hat{\mathbf{n}}$ and the pulling direction [15].

The origin of the surface tension anisotropy is the underlying crystalline structure of the growing solid. Growth is preferred along the crystalline axes and, in two dimensions, a seed grain will typically grow outward as a four-armed “snowflake”. In directional solidification, in which growth is forced along a particular direction, the arms or dendrites are tilted in a direction between the crystalline axis and the imposed temperature gradient.

The effective in-plane anisotropy depends not only on the crystal itself, but also on the orientation of the crystal with respect to the growth direction. When grown in the $\{111\}$ plane, the surface tension is nearly isotropic, leading to seaweed growth or DBM [15].

Mathematically, the surface tension can be represented in 3D as

$$\gamma(\hat{\mathbf{n}}) = \gamma_0 [1 + \epsilon_0(n_1^4 + n_2^4 + n_3^4)] \quad (2)$$

where γ_0 is the isotropic part of the surface tension and ϵ_0 is the degree of anisotropy [15]. The anisotropy has been measured as $\epsilon_0 = 0.0055$ in SCN [16]. $n_1, n_2,$ and n_3 are the components of a unit vector $\hat{\mathbf{n}}$ that parametrizes the function in three dimensions. $\gamma(\hat{\mathbf{n}})$ is the magnitude

*Electronic address: utter@phy.duke.edu; Present address: Dept. of Physics, Box 90305, Duke University, Durham, NC 27708

†Electronic address: eb22@cornell.edu

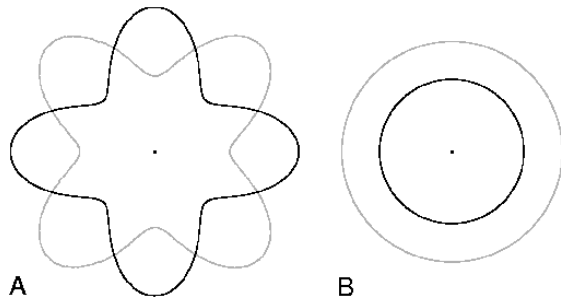


FIG. 1: Using equations 1 and 2, the surface stiffness (grey, $\gamma_0=2$, $\epsilon_0=0.1$) and the anisotropic part of the surface tension (black, $\gamma(\hat{\mathbf{n}}) - \gamma_0$, with $\gamma_0 = 1$ and $\epsilon_0=2.75$) are shown for the (A) $\{100\}$ and (B) $\{111\}$ planes. There is significant fourfold anisotropy in the $\{100\}$ plane while growth in the $\{111\}$ plane is isotropic. Note, the parameters γ_0 and ϵ_0 are chosen to emphasize the anisotropy in the surface tension.

of the surface tension for a surface oriented so that its normal is along $\hat{\mathbf{n}}$. This approximation of the actual surface tension looks somewhat like a rounded cube in three dimensions for succinonitrile and has the expected sixfold symmetry for a cubic crystal.

In directional solidification, the sample is constrained to grow within a particular plane, so the possible growth surfaces have orientations $\hat{\mathbf{n}}$ perpendicular to the interface and lying in the plane of the sample. Constraining $\hat{\mathbf{n}}$ to lie in a plane is equivalent to taking a particular slice through this 3D surface tension plot. Changing the orientation of the crystal changes the shape and magnitude of $\gamma(\hat{\mathbf{n}})$ and $\tilde{\gamma}(\hat{\mathbf{n}})$ in the sample plane [17].

Figure 1 shows examples of these 2D slices in the $\{100\}$ plane and the $\{111\}$ plane. In these cases, the surface stiffness (grey) has the same symmetry as the surface tension (black). They are 90° out of phase and fingers tend to grow towards maximum surface tension. If a crystal in this orientation was forced to grow upwards, Fig. 1A would produce stable dendrites with sidebranches at approximately right angles. We could also rotate the sample (and hence the surface tension plot) in the plane to produce tilted dendrites. Without anisotropy of surface tension, Fig. 1B, the tip is unstable and the growth lacks the apparent orientation observed in traditional growth morphologies.

Figure 2A and B show experimental pictures of solids oriented approximately as shown in Fig. 1A and B respectively. Seaweed structures (2B) are very disordered compared to more familiar arrays of cells and dendrites (2A). Note that Fig. 2A and B show different seed crystals of the same sample grown under the same growth conditions, illustrating that it is the crystalline orientation that causes the observed difference.

Although there have been a couple thorough experimental investigations of the seaweed morphology in directional solidification[15, 17], very little work has been

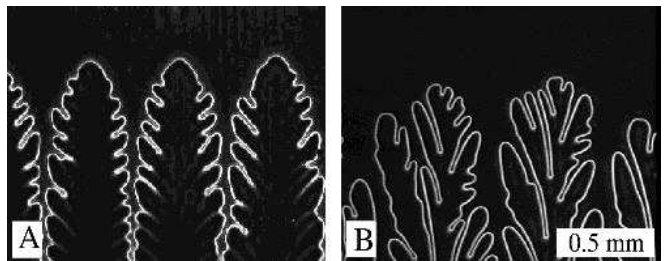


FIG. 2: (A) A dendrite and (B) seaweed structure which differ only in crystalline orientation. The white line indicates the solid-liquid interface. The solid grows upwards into the undercooled melt. The thermal gradient (18 K/cm), concentration (0.25% SCN-PEO), and growth velocity ($2.71 \mu\text{m/s}$) are identical in both pictures.

done on the tip dynamics and the effect of the small misorientations from the $\{111\}$ plane that are present in any experimental study.

Previous experiments and simulations on the seaweed morphology have focused on the magnitude of the anisotropy, stability of dendrites, and the orientation of anisotropic crystals. In particular, Akamatsu and Faivre have performed directional solidification experiments studying the effect of surface tension anisotropy and grain orientation on morphology[15, 17]. Ihle and Müller-Krumbhaar have used numerical simulations to study seaweeds[4], including the seaweed-dendrite transition with increasing anisotropy. Attempts to vary the anisotropy in simulations [4] and experiments [18, 19] showed that tip splitting growth was found when noise was increased.

Brener *et al.* propose a morphology diagram involving the degree of anisotropy and the undercooling [20]. In this diagram, they distinguish between seaweed structures at low anisotropy and dendritic structures at high anisotropy and between fractal growth at low undercooling and compact growth at large undercooling. They theorize that the fractal structure forms because tip splitting occurs randomly when the strength of the thermal noise is large enough to destabilize the tip [20, 21].

Honjo *et al.* claimed the first DLA-like crystal growth using NH_4Cl crystals radially grown from solution and found a fractal dimension $D_f = 1.671$ with about 1 order of magnitude in length scales [18]. Ihle and Müller-Krumbhaar have used numerical simulations to study seaweed morphology and find $D_f = 1.70 \pm 0.03$ [4]. Müller-Krumbhaar *et al.* reconfirmed these results, $1.66 \leq D_f \leq 1.73$, for a seaweed growth at low undercooling [22]. Honjo *et al.*'s results were performed for seaweeds at a particular undercooling and therefore do not test Brener's predictions of a transition to compact growth with increased undercooling. Ihle and Müller-Krumbhaar used three undercoolings and found the fractal dimension to be approximately constant. Their scaling range is not more than one decade and simulations are performed at zero imposed anisotropy which we are not

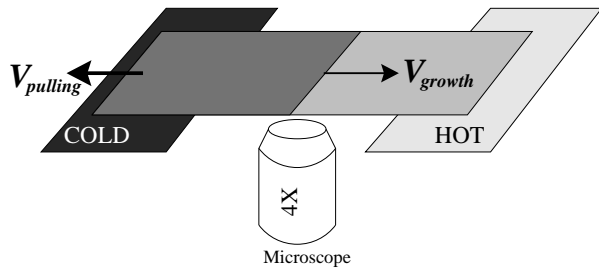


FIG. 3: Directional solidification schematic. A quasi-2D sample is pulled through a linear temperature gradient. The growing interface is stationary in the lab frame and is observed through a microscope.

able to obtain experimentally. Simulations by Sasikimar and Sreenivasen show an increase in fractal dimension from 1.6 to 2 with increased undercooling [23]. Our results suggest a transition from fractal to compact growth, but we find that there is not a significant range of fractal scaling.

At higher anisotropies, the noise is no longer able to destabilize the tip, but might still be important in inducing sidebranching. Dynamic studies of the seaweed morphology might offer more information about the role of noise in solidification.

No systematic study has been concerned with the dynamics of the tip splitting events or the effect of misorientations from the $\{111\}$ plane. This seems particularly important in dense branching morphology as slight misorientations lead to finite anisotropies to the nominally isotropic case. In contrast, slight variations on an anisotropic growth such as that in Fig. 1A would likely be weak. We discuss the implications of these misorientations below.

Low anisotropy systems can be very instructive in understanding the transition from seaweeds to dendrites. This might be particularly important for situations where competing anisotropies nearly balance, such as cases where the kinetic anisotropy favors a different direction than the surface tension anisotropy [24, 25].

This paper is organized as follows: In Section II we describe the experimental apparatus and techniques. In Section III A, we characterize three different types of seaweed growth which result from small anisotropies. In III B, we study the fractal dimension of the degenerate seaweed. In Section III C we study seaweed-dendrite transitions for low anisotropy growth. We conclude in Section IV.

II. EXPERIMENTAL METHODS

The experiment is performed with a traditional directional solidification apparatus [26] in which a thin sample ($13\text{ cm} \times 1.5\text{ cm} \times (5 - 60)\ \mu\text{m}$) is pulled through a linear temperature gradient at a constant pulling velocity as shown in Fig. 3. After an initial transient, the aver-

| | SCN-ACE | SCN-CAM | SCN-PEO |
|-------------------------------|-------------------|-------------------|---------|
| $D\ (\mu\text{m}^2/\text{s})$ | 1270 ^a | 300 ^b | 80 |
| k | 0.1 ^a | 0.33 ^c | 0.01 |
| C (weight %) | 1.5% | 1.3% | 0.25% |
| d (μm) | 20 | 22 | 60 |

TABLE I: Properties of samples used in this study. Succinonitrile (SCN) alloys with acetone (ACE), camphor (CAM) and poly(ethylene oxide) (PEO) as solutes. Diffusivity D and partition coefficient k are given. Solute concentration C and sample thickness d used in these results are also listed. *a)* Reference [30]. *b)* Reference [31]. *c)* Reference [32].

age speed of the solidification front is equal to the pulling speed, set by a linear stepping motor with 4 nm step size.

The cell consists of two glass plates glued together and filled with the sample. The glass plates are cleaned in stages using detergent, acetone, methanol, an acid solution (sulfuric acid and NoChromix (Godax Laboratories, Inc.)), and distilled water. The glue used is the epoxy Torr-Seal (Varian Vacuum Products). The nominal cell depth is set by a Mylar (DuPont) spacer which can be obtained in a wide range of thicknesses with good uniformity.

In each set of runs, the temperature gradient is maintained at a fixed value between 3 and 50 K/cm with a stability of ± 2 mK possible on each side. The temperatures of the hot and cold sides are above and below the equilibrium melting temperature of $\approx 58^\circ$ so that the solid-liquid interface remains within the gap between the temperature controlled blocks. In the most recent design, circular samples are used to allow the cell to be rotated within the sample plane between runs. This allows for some control over sample orientation.

The sample used is an alloy of succinonitrile (SCN) and a small amount of added solute. The solutes used in the present study are either 0.25% poly(ethylene oxide) (PEO)[27], 1.5% acetone (ACE), or 1.3% camphor (CAM). The diffusivities D and partition coefficients k are listed in Table II with the solute concentrations C and sample thicknesses d used for these results. The SCN is purified by sublimation and the samples are mixed, degassed, and vacuum filled under inert atmosphere to avoid possible contamination. The melting temperature of the purified material is $58.05 \pm 0.03^\circ\text{C}$ which corresponds to a purity of 99.98% [28]. Further details on sample preparation and cell construction will be presented elsewhere [29].

The liquid-solid interface is observed with phase contrast or Hoffman modulation contrast microscopy. Sequences of images are recorded using a CCD camera with a framegrabber or time lapse video. Particularly with phase contrast images, such as those in Fig. 2, the interface can then be easily extracted for further analysis.

To initiate growth, the sample is melted completely and quenched, seeding a number of grains. One grain with the desired orientation is selected and all others

are melted off so the chosen grain can grow and fill the width of the cell. This is most easily accomplished in SCN-PEO samples since the attached dye group on the poly(ethylene oxide) [27] allows us to melt off undesirable grains by locally heating with an argon laser beam. The selected grain can then be maintained so runs of different growth speeds can be performed at the same crystalline orientation.

It is important to start with a single grain since dendrites grow at lower undercooling and typically overtake seaweeds during solidification. It is common after a run to have a few subgrains indicating that neighboring lobes can shift slightly with respect to each other[15]. We don't observe any variation in growth morphology after the initial transient due to the formation of these subgrains.

Before each run, the sample is kept stationary ($V = 0$) for a sufficient time to equilibrate the impurity concentration in the liquid and create a flat interface. This allows accurate measurement of the initial instability wavelength of the flat interface λ_f which results from the Mullins-Sekerka instability [33].

Finding an appropriate grain is an experimental challenge, as the random seeding process gives only a 1/1600 chance of orienting the grain within 1° of the $\{111\}$ plane [34]. It has already been noted that seaweeds exist only within 5° of the $\{111\}$ orientation[15]. This 5° limit likely depends on the alloy and concentration used, which appear to affect the degree of anisotropy in our observations. However, assuming that limit of seaweed stability, there is a probability of 1/66 to seed seaweed growth but only 1 in 25 seaweeds will be within 1° of the $\{111\}$ plane. That is, experimental seaweed growths typically involve a significant misorientation from the $\{111\}$ plane. The consequences of this will be emphasized below.

III. RESULTS

A. Seaweed morphologies

Although low anisotropy solidification produces complicated meandering patterns compared to dendrites, we find noticeable regularity due to the imposed growth direction and small anisotropies.

There does appear to be a typical spacing between the large seaweed cells [17], as seen in Fig. 4. This spacing is comparable to that for dendrites grown at the same conditions (e.g. as in Fig. 2), but is unstable and continuously changes over time. There is frequent tip splitting and competition between lobes which are occasionally created or fall behind. The splitting events also occur at different places on the tip and create arms of varying lengths. These factors lead to the characteristic meandering and random appearance of the seaweed.

Given that it is unlikely to randomly seed a seaweed grain within 1° of the $\{111\}$ plane as mentioned above, we must ask how growth is affected by small misorientations from the $\{111\}$ plane. Fig. 5 shows a few possible

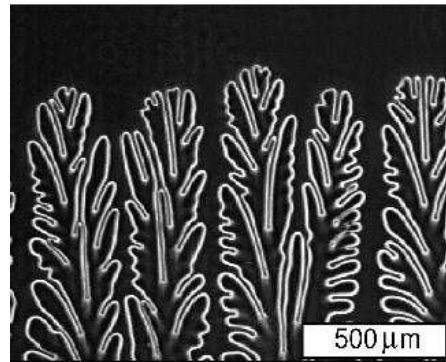


FIG. 4: Seaweed growth in 0.25% SCN-PEO at $V = 6.74 \mu\text{m/s}$. The growth is composed of seaweed cells, five of which are seen here.

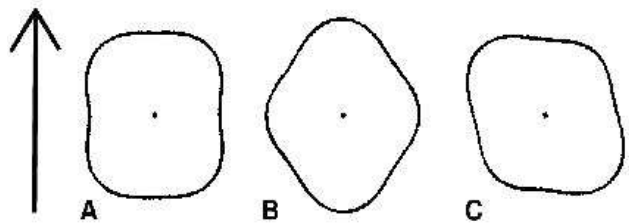


FIG. 5: Anisotropic part of surface tension in planes oriented 5° from the $\{111\}$ orientation using the same parameters as in Fig. 1. (A) Close to the $\{655\}$ plane and (B) near $\{665\}$ orientation. Note that specifying the plane does not select the orientation with respect to the growth direction (given by the arrow). (C) is a specific orientation found by rotating (B) in the sample plane.

surface tension profiles for grains misoriented 5° from the $\{111\}$ plane towards the $\{100\}$ or $\{110\}$ orientation and with in-plane rotations. Not only is the surface tension anisotropic, it is also not generally fourfold symmetric as usually assumed in simulations and theory. Since the grains in Fig. 5 are close to $\{111\}$, the growth will be *relatively* isotropic and should form seaweeds. However, the dynamics of the seaweed will depend on the slight anisotropy.

This effect may be particularly relevant because a slight anisotropy on a nominally isotropic case will break the symmetry and induce a sense of orientation. Slight misorientations from a strongly anisotropic case like the $\{100\}$ orientation will induce only small changes on the existing profile and will not be significant.

In particular, if we force a crystal oriented as Fig. 5A to grow upwards, there will be a small degeneracy [35]. Growth towards the surface tension maxima is preferred and a tip will tend to grow outwards in both directions leading to a marked increase in radius or flattening of the tip. We call this the degenerate seaweed as there is a small amount of degeneracy which is revealed in the dynamics. Forcing a crystal oriented as in Fig. 5B to grow upwards, the seaweed now grows along a preferred

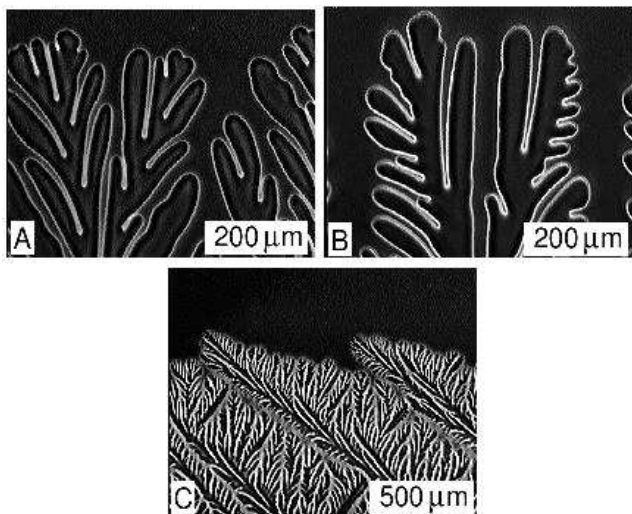


FIG. 6: Three kinds of seaweed growths observed in an SCN-ACE sample at a temperature gradient of 20 K/cm. (A) A degenerate, or alternating tip splitting, mode at $V = 8.96 \frac{\mu\text{m}}{\text{s}}$, (B) a stabilized seaweed at $V = 8.96 \frac{\mu\text{m}}{\text{s}}$ and (C) a strongly tilted seaweed (tilted beyond 45°) at $V = 43.6 \frac{\mu\text{m}}{\text{s}}$ which reveals a twofold rather than fourfold symmetry.

direction and the tip will be somewhat more stable than the isotropic seaweed. This is the stabilized seaweed. Fig. 5C shows the same crystal in Fig. 5B rotated within the plane. As we show below, in this case upward growth can lead to seaweeds tilted beyond 45° as a consequence of the twofold symmetry.

Figure 6 shows a few examples with orientations similar to those shown in Fig. 5. In each case, the same sample is used, but each image corresponds to grains of different crystalline orientation. They are all seaweeds because the tip is unstable to splitting, but there is a clear qualitative difference in their structure. We describe these further below.

1. Degenerate seaweed, alternating tip splitting

One of the most striking types of seaweeds is the degenerate seaweed seen in Fig. 2B and Fig. 6A. At first glance, they appear similar to other seaweeds, except that the tip is observed to alternately split on the left and right sides [14, 36]. That is, when the tip splits, one of the two new lobes will grow forward as the other falls behind. If the lobe towards the left survives, when the tip splits next, there is roughly an 85% chance that the lobe on the right will survive.

We have characterized this state in detail [14], including a model which captures the observed scaling behavior; The tip splitting frequency f , the wavelength of the tip instability λ_t , and the pulling speed V are related as: $f \propto V^{3/2}$, $\lambda_t \propto V^{-1/2}$, and $f \propto \lambda_t/V$. The observed frequency exponent of 3/2 is identical to what is expected for the sidebranching frequency in dendrites[37, 38]. The

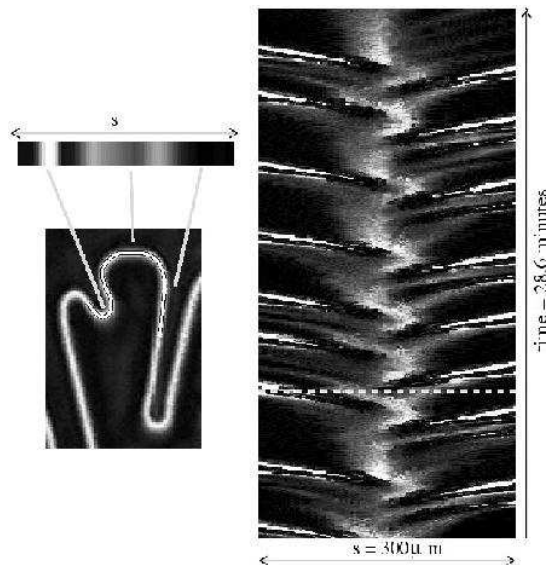


FIG. 7: Curvature-time plot for 0.25% SCN-PEO. A representation of the curvatures along the interface near the tip. To the left is a tip region with an segment indicated in white. Above it, the absolute curvatures along this segment are plotted in greyscale. Stacking sequences of these lines in time for subsequent pictures gives the curvature-time plot on the right, where the center line always corresponds to the tip. Time increases upwards (total time 28.6 minutes). The width is 300 μm and the growth velocity is $2.03 \frac{\mu\text{m}}{\text{s}}$. White corresponds to high curvatures (radius of curvature less than $\approx 10 \mu\text{m}$) and black to zero curvature. The dashed line indicates the position of the tip that is shown.

relevant results will be summarized briefly to contrast with other types of seaweeds and to correlate the previous observations with the surface tension plots shown above: (a) tip splitting can regularly alternate, (b) the instability wavelength of tip splitting is linearly related to the instability wavelength of the planar interface, and (c) alternating tip splitting is correlated with a strong flattening of the tip and a particular crystallographic orientation.

To gain additional insight, the curvature is measured at each point on an arc centered on the tip. Plotting curvature versus the position along the arc and stacking the plots from successive times, we created curvature time (CT) plots, as shown in Fig. 7. The arclength s is centered on the tip which is defined as the furthest point along the growth direction. The greyscale intensity corresponds to the absolute value of the curvature. This plot shows the evolution of the curvatures in the region of the tip over time. The center of the plot always corresponds to the tip. Each splitting event is represented by a double line because a deep groove and an additional tip are created, both of which have high curvature and convect down the side of the seaweed.

The alternating tip splitting can be very regular as seen in Fig. 7. There, it is clear that the curvatures at the tip oscillate, reflecting the alternating flattening and

splitting of the tip. We emphasize that the periodicity seen in Fig. 7 is a reflection of the changing shape of the tip and not an artifact of the tip moving from side to side since the tip position changes by a relatively small amount. This is striking because in a relatively isotropic system with a noise dominated instability such as tip splitting, one expects to find random and unpredictable behavior. Although there could be a nonlinear feedback mechanism that leads to an instability such as vortex shedding in fluid flows, simulations of isotropic solidification have not revealed such a cycle. Although rare, this state is not unique, as we have observed it in three different samples and it appears to be the quasi-periodicity pointed out in Fig. 20 of [15].

Measurements of the tip instability wavelength λ_t versus the instability of the initially flat front λ_f demonstrated an approximately linear relationship. This indicates that to a first approximation, the instability wavelength of tip splitting arises from the more familiar instability of the flat interface. The precise relationships for two particular degenerate seaweed grains show that λ_t is in fact smaller than λ_f ($\lambda_t \approx 0.8\lambda_f$) [14]. The tip will become unstable at the smallest instability wavelength, since the tip is initially at a size that is too small to support an instability and grows. That is, λ_t is essentially probing the small wavelength branch of this dynamic stability curve. The evolving tip is more complicated than the initial planar instability which is itself more complicated than the steady state linear theory of Mullins and Sekerka [33]. Despite this, we find within experimental errors that all of these lengths scale in the same way as $\lambda \propto V^{-0.5}$.

The observed flattening of the tip is precisely what we might expect if the crystal was oriented as Fig. 5A. To verify that this is the case, we performed a run at a very small temperature gradient so that the growth would be dominated by any crystalline anisotropy rather than the imposed temperature gradient. With a reduced temperature gradient, the resulting growth is closer to that of free growth. Figure 8 shows a space-time (ST) plot from the run (see [15], for example). It was created by taking the pixels from a fixed distance behind the interface from each image and stacking them sequentially in time (similar to the CT plot). The distance behind the interface in this figure is $\approx 12\lambda_f$. The plot is essentially a chart recording of the growth in the absence of further coarsening. It's clear that the growth locks into two particular directions, consistent with the surface tension profile shown on the right.

A state qualitatively similar to this alternating tip splitting is observed in viscous fingering experiments, but is due to an additional perturbation, such as the presence of a bubble trapped at the tip [39]. Park and Homsy also see a near periodic splitting, although there is not a long enough sequence to be sure [40]. Alternating tip splitting can also be observed in simulations when competing anisotropies balance [25, see Fig. 3c]. This might result from a slight degeneracy in a relatively isotropic surface

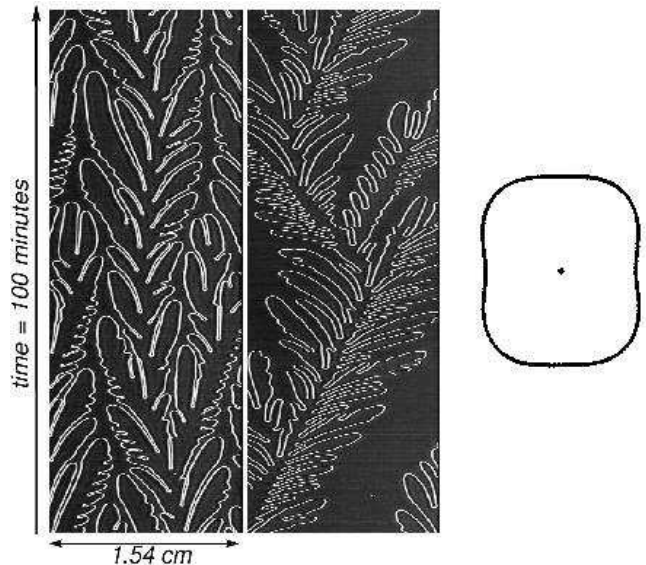


FIG. 8: Space-time plot for 0.25% SCN-PEO degenerate sample. Time increases upwards. The growth velocity is $2.71 \mu\text{m/s}$ and temperature gradient is (A) 18 K/cm and (B) 3 K/cm . The approximate orientation of the grain is represented by the surface tension plot on the right. This is the same grain as Fig. 2B.

tension profile as we believe these results show.

At low speeds, the seaweed cells become more stable and lead to a deviation from the observed $f \propto V^{1.5}$ scaling. Also, the slight asymmetry in the anisotropy is revealed and splitting events to one side dominated the splits to the other. At higher speeds, the structures become smaller and growth is more three dimensional, making it difficult to extract the interface and follow the tip.

2. Stabilized seaweed

Fig. 6B shows the stabilized seaweed. Note that it is the same sample as the degenerate seaweed in Fig. 6A growing at identical conditions except for the orientation of the crystal. Unlike the degenerate seaweed, the tip is not generally splitting towards alternate sides. In fact, the horizontal branches (for example, on the rightmost tip) are true sidebranches which develop below the tip, and the tip splitting is much less frequent.

In Fig. 9, tip curvature is plotted versus time for typical examples of the degenerate and stabilized seaweed. The radius of curvature of the tip is determined as a function of time where the tip is again defined as the furthest point along the growth direction. The curvatures in each case are normalized by the average for the run. It's clear that the standard deviation is smaller for the stabilized seaweed which confirms that the tip exhibits less variation in curvature, suggesting that this might be an example of the situation shown in Fig. 5B. In contrast,

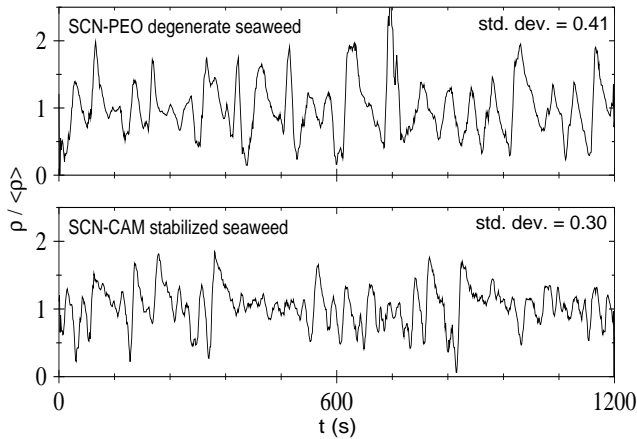


FIG. 9: Curvature of the tip ρ for a (A) degenerate seaweed ($V = 2.71\mu\text{m/s}$, $G = 18\text{K/cm}$) and a (B) stabilized seaweed ($V = 4.5\mu\text{m/s}$, $G = 18\text{K/cm}$). In each case, the curvatures are divided by the mean for the run $\langle\rho\rangle$. The standard deviation for the stabilized seaweed (0.30) is smaller than that for the degenerate seaweed (0.41) reflecting the increased stability of the tip.

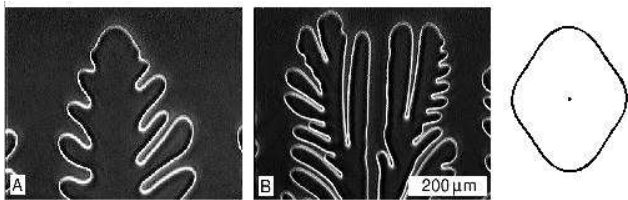


FIG. 10: Tip stabilized seaweed at (A) $V = 4.5\mu\text{m/s}$ and (B) $V = 8.96\mu\text{m/s}$. Both images are 1.5% CN-ACE with $G = 20\text{K/cm}$.

the degenerate seaweed displays prominent oscillations in curvature reflecting the continual splitting and flattening of the tip.

Using a lower pulling speed, the unstable seaweed growth undergoes a transition to dendrites, shown in Fig. 10. The resulting growth seen in Figure 10A shows one of an array of dendrites with stable tips, indicating an anisotropy along the growth direction consistent with the stabilized seaweed. Note that this is not simply an artifact of the temperature gradient constraining the growth, although that might contribute to the stability of the dendrites. At corresponding low velocities, the degenerate state described above appears cellular but remains unstable to splitting.

This effect does not appear to be caused by kinetic anisotropy which generally refers to an increase in anisotropy with increasing velocity. In fact, this is the opposite effect. Qualitatively, this could be interpreted as the same behavior found in simulations in which competing anisotropies balance [41, see Fig. 2 in which decreasing undercooling (2b to 2a) leads to more ordered growth] [42], but we do not believe anisotropies in different directions exist in the present experiment. We also observe

this grain to appear seaweed-like up to $V = 86\mu\text{m/s}$ so there does not appear to be another anisotropic state that dominates at large growth speed. With this in mind and given the evidence in Fig. 9, we conclude that there is a small anisotropy along the growth direction.

It is interesting to note that fractal dendrites described by Brener *et al.* appear very similar [21, see Fig. 5]. In fractal dendrites, although a central stem of the dendrite is still definable, large noise or low anisotropy leads to occasional tip splitting.

3. Strongly tilted seaweeds

The degenerate and stabilized seaweeds are, in a sense, the two extremes of what surface tension profiles will be seen when misoriented from the $\{111\}$ plane. Other growths will be combinations of these behaviors with the additional freedom to rotate the sample in the plane.

Now considering Fig. 5C, the surface tension is not fourfold symmetric. In other words, the model of surface tension based on Eqs. 1 and 2 used most often in simulations and theories, $\gamma(\alpha) = \gamma_0[1 + \epsilon_0 \cos(4\alpha)]$, is not valid here. The lack of complete fourfold symmetry has been noted before [16, 43] but is not typically important for dendrite growth. One consequence is that we can see dendrites growing at angles larger than 45° with respect to the pulling direction, which does not happen under the assumption of fourfold symmetry. If the anisotropy is fourfold symmetric, a dendrite growing at $\alpha > 45^\circ$ will have sidebranches at $90^\circ - \alpha < 45^\circ$ in the other direction which will be favored.

Fig. 6C is an example of this in which a tip splitting growth is tilted at approximately 53° , consistent with a surface tension anisotropy oriented like Fig. 5C. This picture shows that twofold symmetry can be important in seaweed growth. A similar observation can be seen in dendrites [15, see Fig. 25] although no mention is made of the implications of the large tilt angle.

In Fig. 11 we show the progression of this strongly tilted seaweed with increasing growth speed. At low speeds there is a slight tilt to the right. As the pulling speed is increased, branches to the left are more apparent until at large enough speeds they dominate the growth. At much larger speeds, the seaweed actually reverts to a slight tilt to the right as seen at low speeds. Although this transition was reproducible, the temperature gradient is far from linear at those speeds and we are not able to draw reliable conclusions from these observations.

The transition is qualitatively different from the cell to dendrite transition in which cells gradually tilt further towards the crystalline axis until the transition to dendrites [44]. In that case, the cells smoothly tilt further towards the crystalline axis, while here the tilted arms grow out from the seaweed with a lifetime that increases with pulling speed until they become stable.

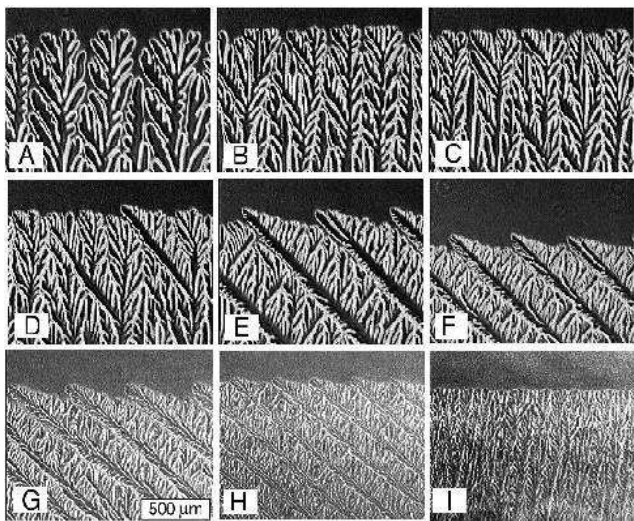


FIG. 11: Transition to strongly tilted growth with increasing growth speed. Images are shown at pulling speeds of (A) 4.5, (B) 9.0, (C) 13.4, (D) 17.8, (E) 22.1, (F) 43.6, (G) 86.4, (H) 182, and (I) 242 $\mu\text{m/s}$. The sample is 1.5% SCN-ACE and $G = 40 \text{ K/cm}$. Images H and I show a transition from strongly tilted seaweed back to growth oriented along the pulling velocity. Although reproducible, the large scale linearity of the temperature gradient is not maintained at $V > 100 \mu\text{m/s}$.

4. Degenerate-stabilized seaweed transitions

From the above discussion, it should be possible to observe transitions between different seaweed types with an in-plane rotation of the sample. Fig. 12 shows an example. At low speeds, a stabilized seaweed forms (12A). When rotated by 30° , the growth becomes a degenerate seaweed and exhibits alternating tip splitting (12B). At higher growth speeds for the same two orientations, stable doublons (12C) become unstable to tip splitting (12D) with the same sample rotation. At the bottom of Fig. 12, possible surface tension profiles are shown which are rotated by 30° with respect to each other. Doublon growth will be addressed in a future publication [45].

B. Fractal dimension

Since we expect to see a crossover from fractal to compact structures with increased pulling speeds [20], we measured the fractal dimension D_f of our images by using a standard box counting method described in Fig. 13 [46]. The lower physical cutoff of the fractal range is close to the wavelength of the initial instability of the flat interface λ_f . The experimental measurement of this value has been measured at each pulling speed and is indicated on the plot (Fig. 13A). D_f is measured as the magnitude of the slope for box sizes $s > \lambda_f$.

Figure 13B shows the fractal dimension versus the pulling speed for a degenerate seaweed. The circles correspond to fitting over one decade on Fig. 13A to determine

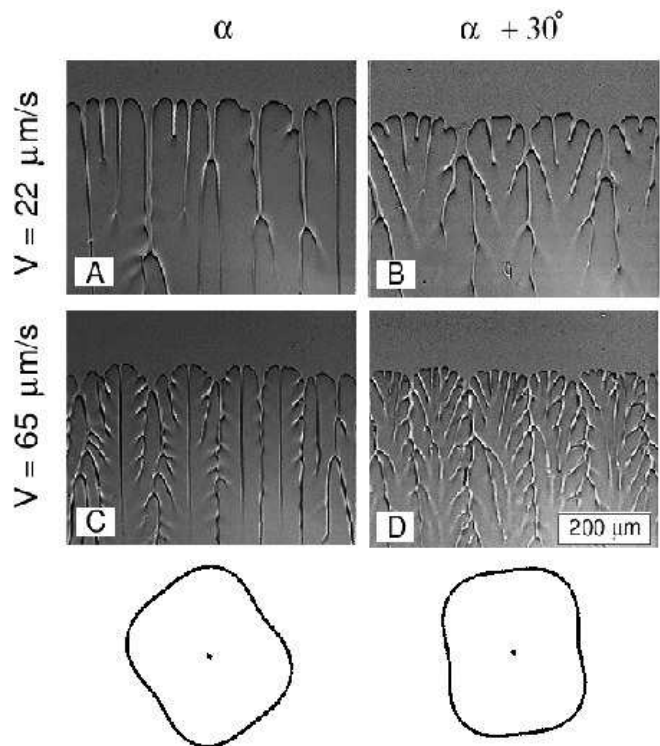


FIG. 12: Transition between stabilized and degenerate seaweed growth with in-plane rotation of sample. The sample is 0.5% SCN-PEO. At a certain sample orientation (α), with (A) $V = 22 \mu\text{m/s}$, the sample grows as stabilized seaweed and at (C) $V = 65 \mu\text{m/s}$ doublons form. After rotating the sample by 30° , the growth becomes (B) a degenerate seaweed at $V = 22 \mu\text{m/s}$ and (D) remains seaweed at $V = 65 \mu\text{m/s}$. Below, possible surface tension profiles are shown which are rotated by 30° with respect to each other.

D_f . The triangles correspond to fitting over 0.43 decades, equivalent to one division on a natural log plot, which has been used in some previous results [4]. It's clear that the fractal dimension is sensitive to the range of data taken for the fit, although the general trend seems to remain that the fractal dimension increases with pulling speed. This increase from close to the diffusion limited aggregation value of 1.67 towards 2 would be consistent with Brener *et al.*'s prediction of a noisy transition from fractal to compact growth. In addition, Brener *et al.* predicted that the transition is discontinuous. When using data from a fit over one decade we observe such a discontinuous jump, however, fitting over a shorter region does not show such a jump. The fit is taken starting at λ_f , i.e. the fit over one decade includes box lengths between λ_f and $10\lambda_f$.

At first, Figure 13B looks promising in indicating a transition from fractal to compact growth, but a few important issues must be noted. As mentioned, the slope is sensitive to the range of the fit and, at most, one decade in length scales can be used. In other words, these pic-

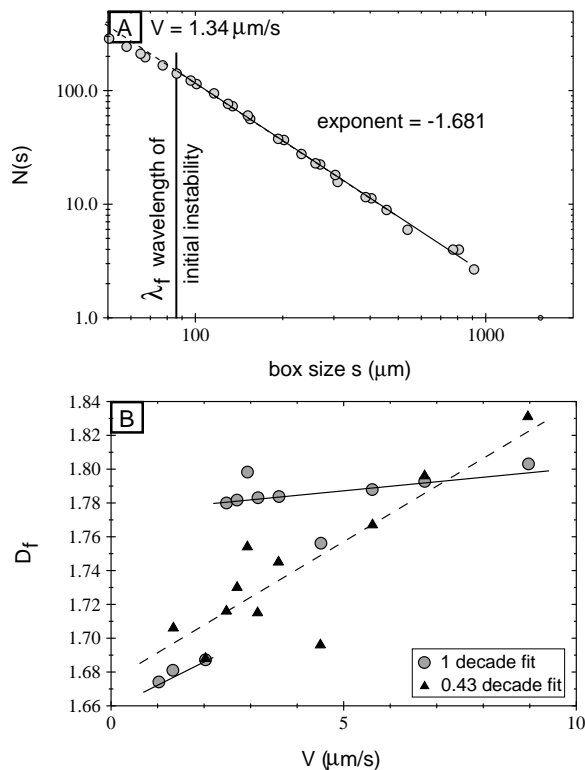


FIG. 13: Fractal analysis for degenerate seaweed (0.25% SCN-PEO). A box counting method is used in which a grid of spacing s pixels is superimposed on a picture of a dendrite and the number of boxes containing any part of the interface ($N(s)$) is counted. (A) A linear region on a log-log plot indicates a fractal range with the dimension given by the magnitude of the slope. The plot here is for a growth velocity of $1.34 \mu\text{m/s}$ and the experimental initial instability wavelength is included as the lower length scale cutoff for the fractal range. (B) Averaging results from 1000 pictures for each point, the fractal dimension versus the pulling speed is plotted. The solid line (circles, 1 decade fit) suggests a discontinuous jump while the dashed line (triangles, 0.43 decade fit) suggests a smooth transition.

tures do not exhibit growth that is clearly fractal over a significant range of length scales. We question whether previous experiments have had the same limitations. At lower speeds, as the seaweed tends towards less developed cellular growth, the calculated dimension actually drops towards one rather than levelling out. The fractal dimension also appears to be most well defined at the tip, as the dimension increases towards 2 when more of the deep groove region is included in the analysis. This could be an artifact of the imposed gradient and may not be an issue in free radial growth where the number of lobes must continually increase.

In summary, our results suggest a transition from fractal to compact growth, but we find that the range of data spans only one decade, making a conclusive interpretation as fractal scaling impossible.

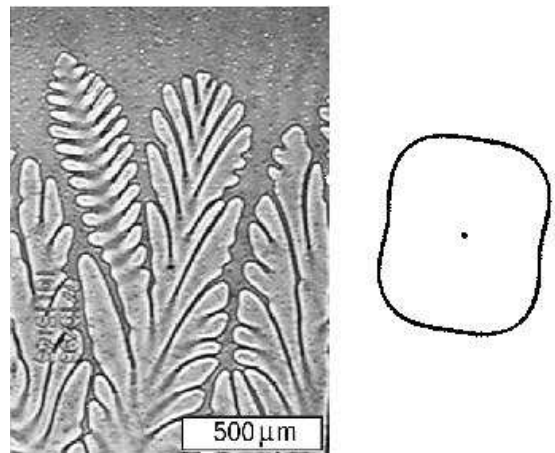


FIG. 14: Dendritic growth from a degenerate seaweed. The approximate orientation of the crystal is inferred to be that represented by the surface tension plot on the right. The sample is 0.25% SCN-PEO growing at $V = 4.5 \mu\text{m/s}$ and $G = 30 \text{ K/cm}$.

C. Seaweed-dendrite transitions

In low anisotropy growth, it is possible to observe dendritic growths in patterns that otherwise are seaweed. For example, Figure 14 shows a snapshot of the alternating tip splitting seaweed that is tilted to the right approximately 9 degrees as represented by the surface tension plot. One of the side branches of the seaweed has nucleated a dendritic branch. Assuming that the anisotropy of the crystal is mirror symmetric, the angle between the dendritic branches would be 43° , which is consistent with the value of 40° for similar branches in Fig. 8B. Due to the regularity of the sidebranches these dendrites look different from the usual dendrites which are observed for growth along the crystal's easy axis. They look very similar to the tip oscillating growth or symmetric tip splitting state of Honjo *et al.*[47]. In their results, the tip velocity and curvature oscillate in time, but these oscillations are not apparent here.

Fig. 15 shows the time evolution of the formation of one of these dendritic branches. The arrow highlights the seaweed arm which becomes dendritic. We also observe in Fig. 14A and Fig. 15E that the dendritic branch grows ahead of the seaweed growth. This is not surprising as it is already known that dendrites grow faster than seaweeds at the same conditions. One might guess that the dendritic arm could grow ahead of the neighboring seaweed and dominate the growth. Indeed, the seaweed growth in this case is not stable – dendritic branches nucleate at different points along the interface and take over the pattern. Both seaweeds and dendrites can be understood as two stable states with dendrites being dynamically preferred over seaweeds. The seaweeds are typically found to be stable until the first dendrites are formed. An example of the the evolution of the seaweed to dendrite transition is shown in Fig. 16. There, an initial seaweed

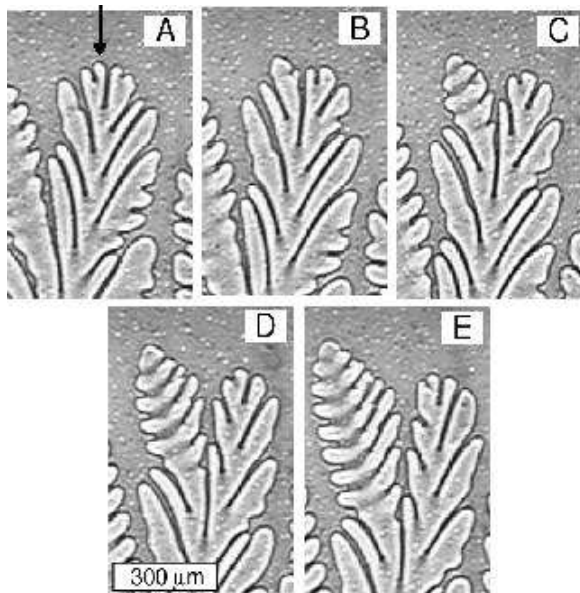


FIG. 15: The formation of a dendritic growth like that shown in Fig. 14. The arrow indicates the seaweed arm that develops into the dendritic branch. The time between pictures is 30 s. The sample is 0.25% SCN-PEO growing at $V = 4.5 \mu\text{m/s}$ and $G = 30 \text{ K/cm}$.

is seen to nucleate dendritic branches. In Fig. 16E, after about 20 minutes of growth, some of the dendrites have managed to grow ahead of the seaweeds.

A seaweed cannot generally overtake a dendrite since it grows at larger undercooling. It is possible though when the dendrite is angled away from the seaweed. Fig. 17 shows a space-time plot in which a dendritic growth appears stable for a long time. After a number of failed attempts, a seaweed branch nucleates on the left and gradually spreads to the right. It is clear from the ST plot that the seaweed grows out from a branch on the dendritic growth and is not simply another grain. Fig. 17C shows the initial formation of the seaweed grain.

IV. CONCLUSION

In conclusion, we find that misorientations from the $\{111\}$ plane lead to different types of seaweeds arising from small anisotropies. These include the degenerate, stabilized and strongly tilted seaweeds. The degenerate and stabilized seaweeds are the two basic types of misorientation with the additional freedom to have in-plane

rotations. The strongly tilted growth in particular highlights the underlying twofold, rather than fourfold, symmetry. The degenerate state is found to allow a regular alternating tip splitting to develop. The observed growth morphologies are correlated with the plots of the in-plane surface tension.

The fractal dimension was studied as a function of growth velocity for the degenerate seaweed. Although

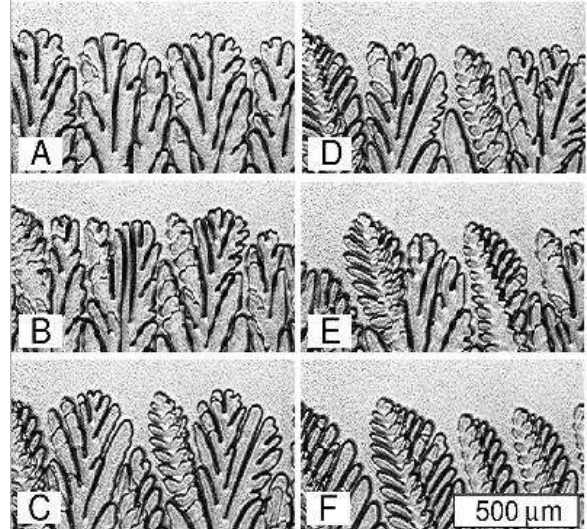


FIG. 16: Transition from a (A) seaweed morphology to a (F) dendritic morphology over time. The pictures are separated by 240 seconds. The sample is 0.25% SCN-PEO growing at $V = 4.5 \mu\text{m/s}$ and $G = 45 \text{ K/cm}$.

we observe a general trend supporting the predicted fractal to compact transition with increasing undercooling, there is not a sufficient scaling region in directional solidification to consider it to be a true fractal. Transitions between seaweed and dendrite growth were also observed.

Ultimately, the question is: How does surface tension anisotropy select particular growth morphologies? In particular, we ask: (i) What can we learn about the crossover between tip splitting and sidebranching with small increasing (non-fourfold) anisotropies? (ii) How can we elucidate the role and identify the relative importance of kinetic anisotropy? and (iii) Are similar morphologies observable in other low anisotropy systems?

This work was supported by the Cornell Center for Materials Research (CCMR), a Materials Research Science and Engineering Center of the National Science Foundation (DMR-0079992).

[1] For reviews, see for example: J. S. Langer, in *Chance and Matter*, edited by J. S. et al. (North Holland, Amsterdam, 1987), pp. 629–711. Y. Saito, *Statistical Physics of Crystal Growth* (World Scientific, New Jersey, 1996).
[2] G. P. Ivantsov, NASA Technical Memorandum 77889,

translated from *Akademiia Nauk SSR, Doklady* **58**, 567 (1947).

[3] M. E. Glicksman, R. J. Schaefer, and J. D. Ayers, *Metallurgical Transactions A* **7A**, 1747 (1976).

[4] T. Ihle and H. Müller-Krumbhaar, *Phys. Rev. Lett.*, **70**,

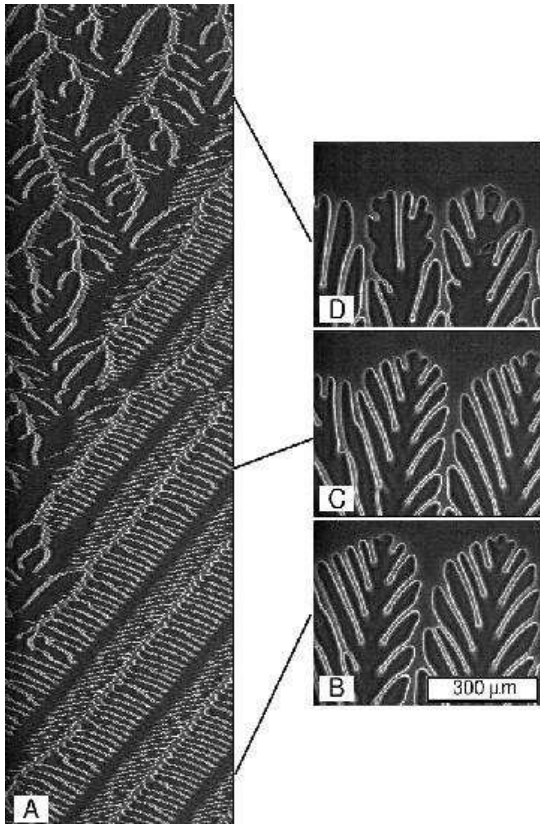


FIG. 17: (A) Space-time (ST) plot of a dendritic interface that undergoes a transition from a (B) dendritic to a (D) seaweed morphology. The discontinuity in the ST plot is due to a translation of the microscope stage along the interface. The sample is 0.12% SCN-CAM growing at $V = 13.4 \mu\text{m/s}$ and $G = 22 \text{ K/cm}$.

- 3083 (1993), Phys. Rev. E, **49**, 2972 (1994).
- [5] E. Ben-Jacob *et al.*, Phys. Rev. Lett. **57**, 1903 (1986).
- [6] K. McCloud and J. Maher, Phys. Rep. **260**, 139 (1995).
- [7] E. Ben-Jacob and P. Garik, Nature **343**, 523 (1990).
- [8] T. Matsuyama and M. Matsushita, Crit. Rev. Microbiol. **19**, 117 (1993).
- [9] J. Wakita *et al.*, J. Phys. Soc. Jpn. **67**, 3630 (1998).
- [10] O. Zik and E. Moses, Physical Review E **53**, 1760 (1996).
- [11] C. H. Shang, Physical Review B **53**, 13759 (1996).
- [12] N. Samid-Merzel, S. Lipson, and D. Tannhauser, Physica A **257**, 413 (1998).
- [13] E. Ben-Jacob *et al.*, Physical Review Letters **55**, 1315 (1985).
- [14] B. Utter, R. Ragnarsson, and E. Bodenschatz, Physical Review Letters **86**, 4604 (2001).
- [15] S. Akamatsu, G. Faivre, and T. Ihle, Physical Review E **51**, 4751 (1995).
- [16] M. Muschol, D. Liu, and H. Cummins, Physical Review A **46**, 1038 (1992).
- [17] S. Akamatsu and G. Faivre, Phys. Rev. E **58**, 3302 (1998).
- [18] H. Honjo, S. Ohta, and M. Matsushita, Journal of the Physical Society of Japan **55**, 2487 (1986).
- [19] H. Honjo, S. Ohta, and M. Matsushita, Physical Review A **36**, 4555 (1987).
- [20] E. Brener, H. Müller-Krumbhaar, and D. Temkin, Phys. Rev. E, **54**, 2714 (1996), E. Brener, H. Müller-Krumbhaar, D. Temkin, and T. Abel, Physica A, **249**, 73 (1998).
- [21] E. Brener *et al.*, Physica A **204**, 96 (1994).
- [22] H. Müller-Krumbhaar, M. Zimmer, T. Ihle, and Y. Saito, Physica A **224**, 322 (1996).
- [23] R. Sasikumar and R. Sreenivasan, Acta Metall. Mater. **42**, 2381 (1994).
- [24] F. Liu and N. Goldenfeld, Physical Review A **42**, 895 (1990).
- [25] T. Ihle, Eur. Phys. J. B **16**, 337 (2000).
- [26] K.A. Jackson and J.D. Hunt, Acta Metallurgica, **13**, 1212 (1965); J.D. Hunt, K.A. Jackson, and H. Brown, Rev. Sci. Instrum., **37**, 805 (1966).
- [27] Poly(ethylene oxide) with an attached rhodamine dye (Sulferhodamine Bis-(PEG 2000), molecular wt. 4500) is purchased from Molecular Probes, Inc. (Eugene, OR).
- [28] See M. E. Glicksman, R. J. Schaefer, and J. D. Ayers, Metallurgical Transactions A **7A**, 1747 (1976). Although the identities of the impurities are not known, an estimate is made using the melting temperature of succinonitrile and the liquidus slope for acetone ($m = 2.8 \text{ K / weight \%}$).
- [29] B. Utter, R. Ragnarsson, and E. Bodenschatz, in preparation.
- [30] M. Chopra, M. Glicksman, and N. Singh, Journal of Crystal Growth **92**, 543 (1988).
- [31] T. Sato, W. Kurz, and K. Ikawa, Trans. Japan Inst. Metals **28**, 1012 (1987).
- [32] T. Taenaka, H. Esaka, S. Mizoguchi, and H. Kajioka, Materials Transactions, JIM **30**, 360 (1989).
- [33] W. W. Mullins and R. F. Sekerka, Journal of Applied Physics **35**, 444 (1964).
- [34] For a sphere of radius 1, the surface area of a cap composed of all points within 1° of a particular vector, e.g. the 111 vector, is $A_1 = 2\pi(1 - \cos(1^\circ)) = 1.52 \times 10^{-4}$. There are 8 such equivalent orientations and the total area of all these caps is $A = 8 \times A_1 = 1.22 \times 10^{-3}$. Taking the probability of randomly selecting one of these orientations to be the ratio of this area to the area of the sphere, we get $P = \frac{A}{4\pi} \approx \frac{1}{1600}$.
- [35] Degeneracy refers to an orientation in which growth along ± 45 degrees relative to the pulling velocity is favored, leading to competition between the two preferred orientations (e.g. when Fig. 1A is rotated by 45° and the growth direction is upwards).
- [36] See reference [15]. In particular, note Fig. 20 which highlights a region of “quasiperiodicity” similar to these results.
- [37] B. Billia and R. Trivedi, in *Handbook of Crystal Growth*, edited by D. T. J. Hurle (North Holland, New York, 1993), No. 1b.
- [38] M. Georgelin and A. Pocheau, Physical Review E **57**, 3189 (1998).
- [39] Y. Couder, N. Gerard, and M. Rabaud, Physical Review A **34**, 5175 (1986).
- [40] C. Park and G. Homsy, Physics of Fluids **28**, 1583 (1985).
- [41] F. Liu and N. Goldenfeld, Phys. Rev. A **42**, 895 (1990). Refer to Figure 2 in which decreasing undercooling (Fig. 2b to 2a) leads to more ordered growth.
- [42] E. Ben-Jacob, P. Garik, and D. Grier, Superlattices and Microstructures **3**, 599 (1987).
- [43] A. Dougherty, Journal of Crystal Growth **110**, 501

- (1991).
- [44] S. Akamatsu and T. Ihle, *Physical Review E* **56**, 4479 (1997).
- [45] B. Utter and E. Bodenschatz, *in preparation* (2002).
- [46] *See for instance*, H. Peitgen, H. Jürgens, and D. Saupe, *Chaos and Fractals*, (Springer-Verlag, New York, 1992).
- [47] H. Honjo, S. Ohta, and Y. Sawada, *Physical Review Letters* **55**, 841 (1985).